GIANT METERWAVE RADIO TELESCOPE OBSERVATIONS OF AN M2.8 FLARE: INSIGHTS INTO THE INITIATION OF A FLARE–CORONAL MASS EJECTION EVENT

PRASAD SUBRAMANIAN[1], S. ANANTHAKRISHNAN[2], P. JANARDHAN[3], M. R. KUNDU[4], S. M. WHITE[4] and V. I. GARAIMOV[4]

[1]*Inter-University Centre for Astronomy and Astrophysics, P.O. Bag 4, Ganeshkhind, Pune 411007, India (e-mail: psubrama@iucaa.ernet.in)*

[2]*National Centre for Radio Astrophysics, TIFR, P.O. Bag 3, Ganeshkhind, Pune 41007, India*

[3]*Physical Research Laboratory, Astronomy and Astrophysics Division, Navrangpura, Ahmedabad 380009, India*

[4]*Department of Astronomy, University of Maryland, College Park, MD 20742, U.S.A.*

(Received 10 June 2003; accepted 23 September 2003)

Abstract. We present the first observations of a solar flare with the GMRT. An M2.8 flare observed at 1060 MHz with the GMRT on 17 November 2001 was associated with a prominence eruption observed at 17 GHz by the Nobeyama radioheliograph and the initiation of a fast partial halo CME observed with the LASCO C2 coronagraph. Towards the start of the eruption, we find evidence for reconnection above the prominence. Subsequently, we find evidence for rapid growth of a vertical current sheet below the erupting arcade, which is accompanied by the flare and prominence eruption.

1. Introduction

We have recently started observing the Sun with the Giant Meterwave Radio Telescope (GMRT) near Pune, India. We report here the observation of an interesting flare-coronal mass ejection (CME) event on 17 November 2001. The event was analyzed using data from the GMRT, the Nobeyama radioheliograph (NoRH) and the Hiraiso spectrograph (HiRAS) in Japan, the Radio Solar Telescope Network (RSTN) in Australia, the Mount Wilson Observatory in the U.S.A. and the Michelson Doppler Imager (MDI) and Large-Angle Spectroscopic Coronagraph (LASCO) on board the Solar and Heliospheric Observatory (SOHO).

We give a brief description of the GMRT and the solar observing procedure in Section 2, followed by a multi-wavelength overview of the flare–CME event in Section 3. We interpret the data in Section 4 and draw conclusions in Section 5.

2. The Giant Meterwave Radio Telescope (GMRT)

The GMRT is located about 80 km north of the city of Pune in Maharashtra, western India (latitude 19°06′ N, longitude 74°03′ E, altitude 650 m). It consists

Solar Physics **218:** 247–259, 2003.

of thirty 45-m diameter antennas spread over 25 km. Half of these are in a compact, randomly distributed array of about 1 km and the rest are spread out in an approximate 'Y' configuration. The shortest baseline is 100 m and the longest is 26 km. GMRT currently operates in the frequency bands around 150, 235, 325, 610, and 1000–1450 MHz. It is among the most sensitive telescopes in the world in these bands and also provides seconds of arc angular resolution (Ananthakrishnan and Rao, 2002). Further details about the GMRT can be found at the URL *http://www.gmrt.ncra.tifr.res.in*.

2.1. Observing the Sun with the GMRT

These observations represent the first attempts at imaging the Sun with the GMRT after most of the antennas had started functioning. Our observing frequencies ranged from 1060 to 1076 MHz. There were 28 antennas working through the duration of the observations presented in this paper. We did not track the Sun continuously during these observations. Instead, we repositioned the antennas at the Sun center every 30 min. Within each 30-min interval, the phase center was allowed to drift. The data were then corrected for solar motion during subsequent data analysis. We typically observed the Sun for around 20 min and the phase calibrator (3C298) for 6–7 min in each 30-min cycle. Solar attenuators of 30 dB were inserted while observing the Sun and they were removed while recording data on the calibrator. Since the GMRT antennas are not yet equipped with extra high noise calibrators (which can generate noise corresponding to ~ 1 s.f.u.) we cannot place much confidence in the absolute values of flux observed at this time. We therefore normalized the fluxes we observed to the peak flux observed by the Nobeyama Radio Polarimeter (NoRP) at 1 GHz (*http://solar.nro.nao.ac.jp/norp/html/daily/*). Since the automatic gain control (AGC) circuits were on throughout the duration of the observations, the flux at the final peak of the flare is somewhat suppressed relative to the preceding smaller peaks (see Figure 8). We used an integration time of 16 s; this is therefore the minimum time cadence with which we can obtain snapshot images for this observation. In principle, it is possible to go down to an integration time as low as 2 s but no lower, because the time constant of the AGC circuits is of the order of 1 s. The data were processed using the standard NRAO/AIPS software. Snapshot images, with a dynamic range of $\simeq 10$, of the flaring region were obtained every 16 s using a restoring beam size of $34'' \times 24''$ in right ascension and declination, respectively.

3. An Overview of the Event

A long-duration M2.8 flare was observed on 17 November 2001 at 1060 MHz with the GMRT. The X-ray flare which originated in NOAA active region 9704 (S18 E41), started at 04:49 UT, showed a smooth rise, peaked at 05:25 UT and exhibited a long decay period before ending at 06:11 UT. The X-ray fluxes observed

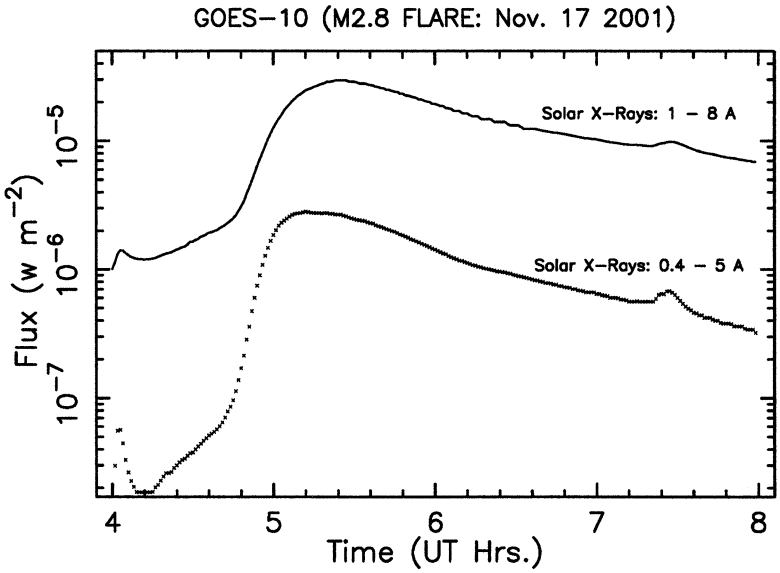

Figure 1. Soft X-ray light curves from the GOES 10 satellite. *Upper curve*: 1–8 Å. *Lower curve*: 0.5–4 Å. The X-ray flare started at 04:49 UT, showed a smooth rise, peaked at 05:25 UT, and exhibited a long decay period before ending at 06:11 UT.

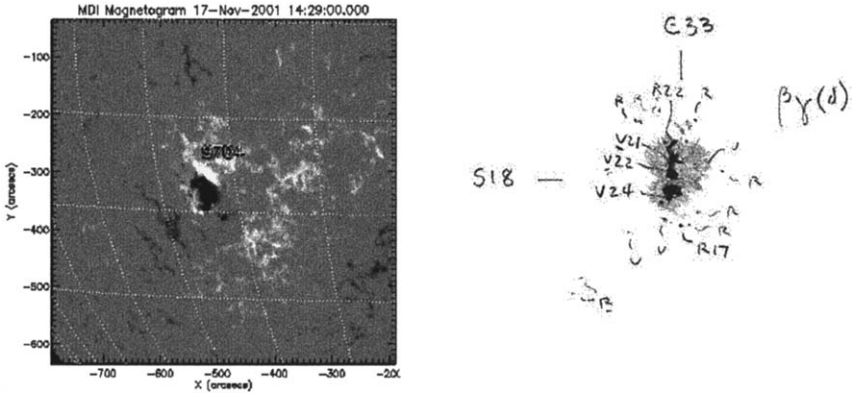

Figure 2. Left panel: the MDI longitudinal magnetogram of AR 9704. The magnetic complexity of AR 9704 is clearly evident. *Right panel*: the Mount Wilson sunspot drawing for this region. The Mount Wilson sunspot drawing on 17 November 2003 assigns a $\beta\gamma\delta$ category to this active region.

by GOES 10 in the 1–8 Å and 0.5–4 Å bands are shown in Figure 1. Figure 2 shows the MDI longitudinal magnetogram of AR 9704 (left panel) and the Mount Wilson sunspot drawing for this region (right panel). An examination of the longitudinal magnetogram shows that it is clearly more complex than a simple bipole. The central black polarity spot is sandwiched by white polarities to its northwest and southeast, suggesting the existence of at least two sets of loop systems. This active region was classified as a β configuration by the *Solar Geophysical Data*

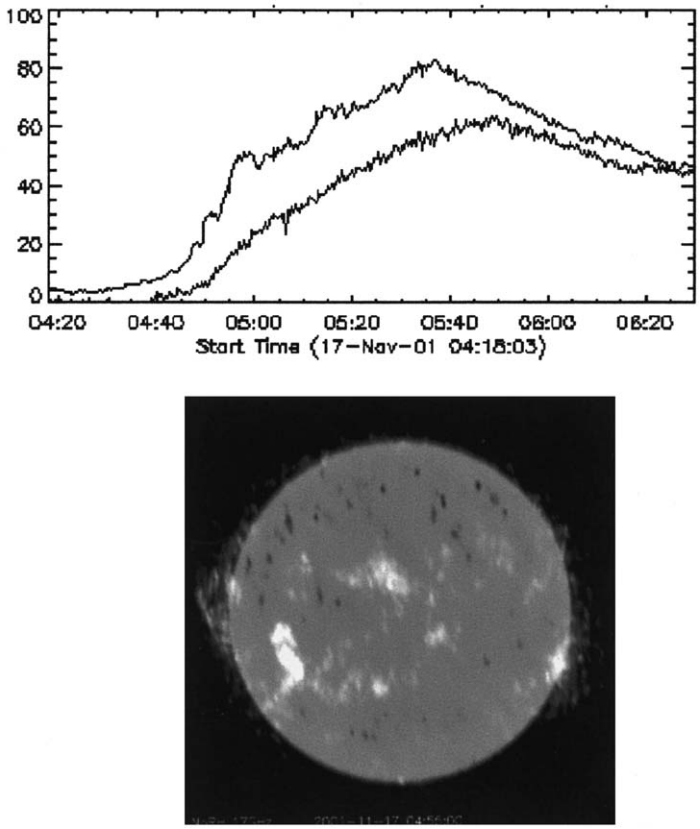

Figure 3. Upper panel: the upper curve is the 17 GHz light curve and the lower curve is the 34 GHz light curve from the NoRH. The vertical axis gives the flux in s.f.u. Both the light curves show a gradual rise and decay, implying that the radiation at these frequencies is thermal in nature. This radiation arises primarily from the active region situated at S18 E40, that is evident in the lower panel. *Lower panel*: image of the Sun at 17 GHz at 04:55 on 17 November 2001 from the NoRH showing the erupting prominence on the east limb. The prominence, which was situated towards the northeast of the thermal active region emission evident at S18 E40, erupted at $\sim$04:48 UT. A movie of this event is available at *http://solar.nro.nao.ac.jp/norh/html/10min/*.

Reports on 17 November 2001, but its complexity was upgraded to $\beta\gamma\delta$ on 19 November 2003, when it had rotated closer to disk center. The Mount Wilson sunspot drawing on 17 November 2003 assigns a $\beta\gamma\delta$ category to this active region. Notwithstanding the disparity between the classifications of AR 9704 on 17 November 2003, the magnetogram and the sunspot drawing provide sufficient evidence for the magnetic complexity of AR 9704. The 1060 MHz GMRT images, described later (see Figure 9) show evidence for two sets of loop systems in this region, providing additional evidence for its complexity.

The flare was accompanied by a fast halo ($\sim$ 1500 km s^{-1}) coronal mass ejection that first appeared in the C2 field of view of LASCO at around 05:30 UT

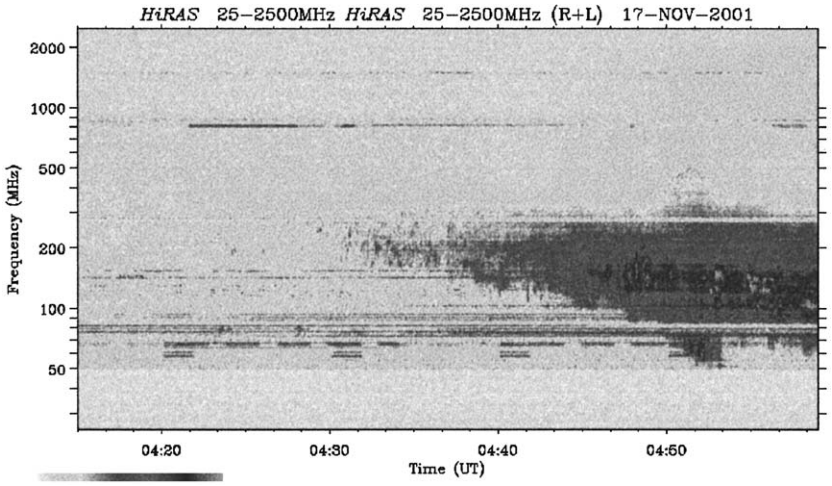

Figure 4. Dynamic spectra from the Hiraiso spectrograph. The start of the continuum emission at ∼ 200 MHz at ∼ 04:35 UT is clearly evident. The lower envelope of the drifting continuum represents the upper end of a feature that is drifting upwards. The height–time profile of this lower envelope is shown in Figure 5.

(*http://cdaw.gsfc.nasa.gov/CME_list*). Figure 3 shows the light curve of the 17 and 34 GHz emission from the NoRH and a representative 17 GHz image from the NoRH that shows the erupting prominence. The bright on-disk emission at 17 GHz evident in Figure 3 is centered at around S18 E40. The 17 GHz emission shows a characteristically gradual rise and decay, indicating that it is thermal in nature at these frequencies. On the other hand, the impulsive nature of the 200, 410, 500, and 1060 MHz light curves (see Figures 6–8) is evidence of their non-thermal nature. The 10-min cadence movie of the 17 GHz data for this event available on the Nobeyama web page (see Figure 3) suggests that the prominence started lifting off sometime between 04:45 UT and 04:55 UT. A detailed analysis of the prominence eruption associated with this event by Kundu *et al.* (2003) establishes that the rapid phase of the prominence lift-off started at around 04:48 UT.

Figure 4 shows dynamic spectrum of the event from the Hiraiso spectrograph. The spectrum shows drifting continuum emission starting at ∼ 04:35 UT at ∼ 200 MHz and drifting downwards in frequency. The lower envelope of this drifting continuum emission represents the upper end of a feature that is drifting upward in the solar corona. The HiRAS dynamic spectrum did not have data below 50 MHz for this event. We were therefore able to follow the lower envelope of the drifting continuum only until ∼ 04:50 UT. An approximate curve was fitted to the lower envelope of the drifting continuum. Using the formulae given by Aschwanden and Benz (1995), the frequency of emission was related to its height in the solar atmosphere assuming that the observed radiation is emitted at the fundamental plasma frequency. Figure 5 shows the results of these computations. It shows the upward

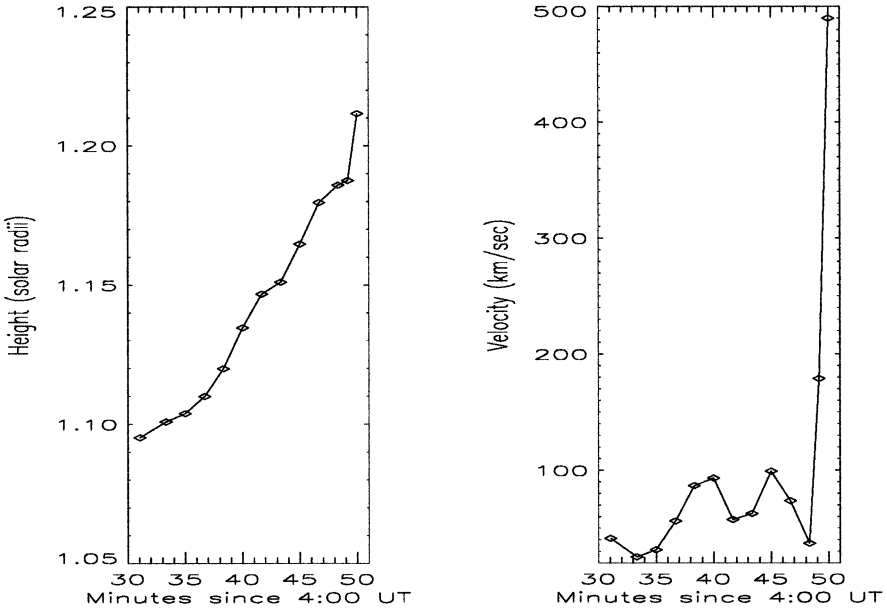

Figure 5. Left panel: the height–time profile of the lower envelope of the drifting continuum evident in the dynamic spectrum of Figure 4. It represents the upper end of a vertical current sheet that forms beneath the erupting prominence. *Right panel*: the velocity–time profile of the same feature. The abrupt increase in velocity at around 04:48 UT can be inferred from the increased curvature around this time of the lower envelope of the drifting continuum (Figure 4).

motion of the feature represented by the lower envelope of the drifting continuum (evident in Figure 4) through the solar corona.

In contrast to the slow rise and fall in the 17 and 34 GHz light curves, the light curves at 200, 410, 500, and 1060 MHz show an impulsive nature. In fact, the 200 MHz emission is the first sign of non-thermal activity associated with this event. Figure 6 shows fixed-frequency light curves at 200 MHz (lower panel) and 500 MHz (upper panel) from the Hiraiso spectrograph while Figure 7 shows the fixed-frequency light curve at 410 MHz from the Radio Solar Telescope Network (RSTN) telescope at Learmonth, Australia. The emission at 200 MHz starts rising at around 04:22 UT while that at 500 MHz starts rising at around 04:50 UT. Figure 8 shows the 1060 MHz light curve derived from the GMRT observations. This emission has three distinct peaks. The largest peak of the GMRT 1060 MHz light curve is normalized to the largest peak of the 1 GHz light curve from the NoRP (*http://solar.nro.nao.ac.jp/norp/html/daily/*). The general shape of the GMRT 1060 MHz light curve is very similar to the NoRP 1 GHz light curve. However, the third and largest peak in the GMRT 1060 MHz data is suppressed relative to the first two peaks, since the AGC circuits were on during the observation. As a result, the ratios peak1/peak3 and peak2/peak3 from the GMRT 1060 MHz light curve are around 50% larger than the corresponding ratios obtained from the NoRP 1 GHz

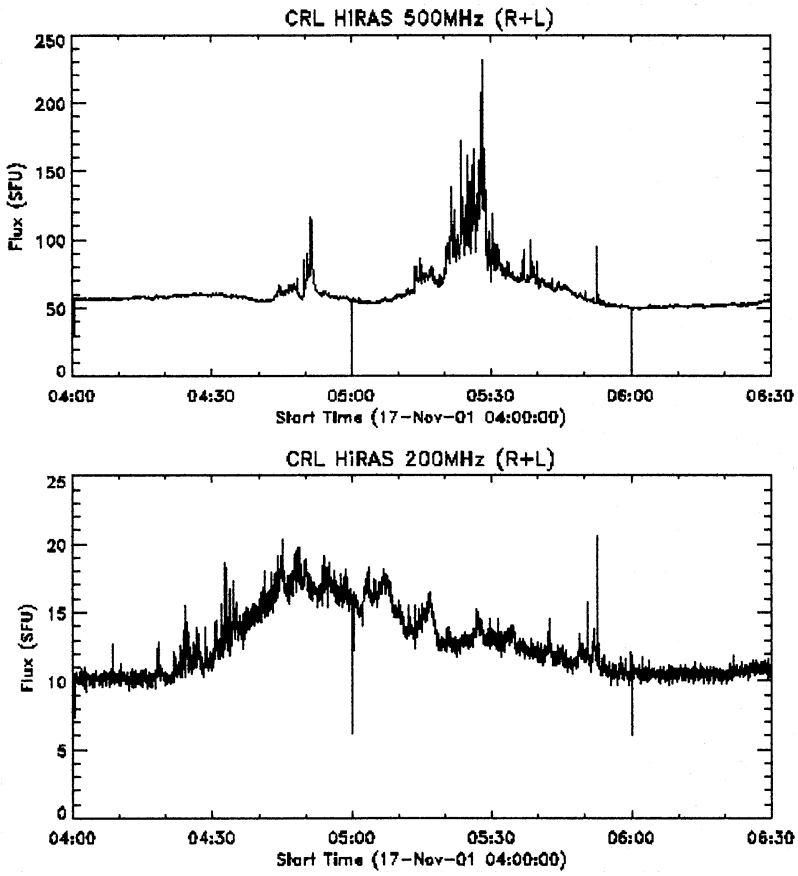

Figure 6. Fixed-frequency light curves at 200 and 500 MHz from the Hiraiso spectrograph. The emission at 200 MHz starts rising at around 04:22 UT while that at 500 MHz starts rising at around 04:50 UT.

light curve. Figure 9 shows 16-s snapshots of the 1060 MHz emission observed with the GMRT. The images are centered at S15 E46, with a field of view of $600'' \times 600''$. The first peak of the 1060 MHz GMRT light curve near 04:52 UT is associated with the brightening of a banana-shaped NS oriented structure near the center of the field of view of the images. The second peak near 05:18 UT is also associated with the brightening of the same structure. The third and strongest peak, at around 05:32 UT, corresponds to a brightening of a NE-SW oriented source to the south of the 'banana'. The brightness temperature of the radiation at each of these three peaks is $\lesssim 10^8$ K, indicating its non-thermal nature. Figure 10 shows 16-s snapshot images near the rising edge of the first peak. The images clearly show that the first peak of the 1060 MHz emission occurred at around 04:48 UT.

The 1060 MHz GMRT images reveal the existence of at least two sets of loop systems (N–S and NE–SW). Together with the magnetograms and sunspot drawing

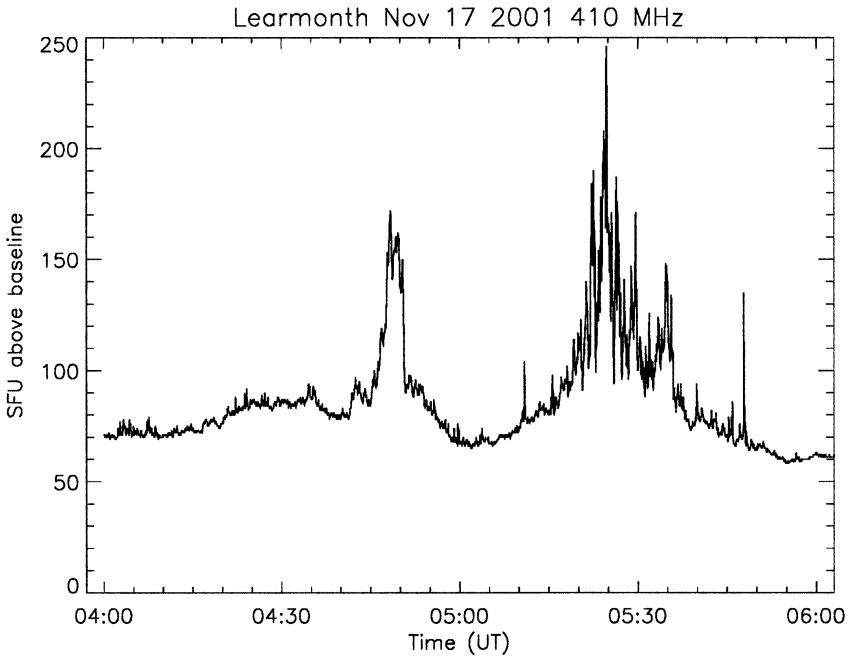

Figure 7. Fixed-frequency light curve at 410 MHz from the Radio Solar Telescope Network (RSTN) telescope at Learmonth, Australia. The vertical axis is calibrated in s.f.u.'s above the baseline.

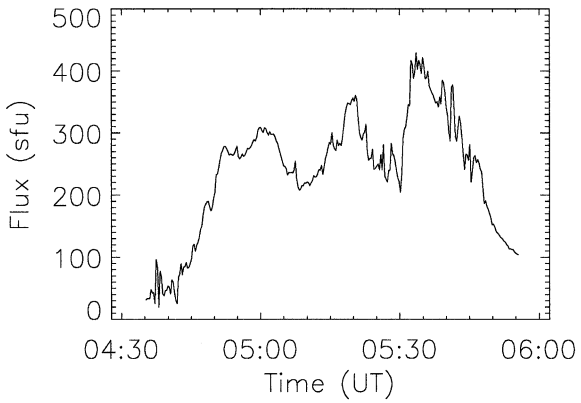

Figure 8. The 1060 MHz light curve from GMRT observations. The three peaks are clearly evident. The first onset of non-thermal emission at this frequency occurs at 04:48 UT. The peak of this light curve is normalized with respect to the peak of the 1 GHz light curve from the NoRP (*http://solar.nro.nao.ac.jp/norp/html/daily/*). Figure 9 shows 16-s snapshot images near the three peaks of this light curve.

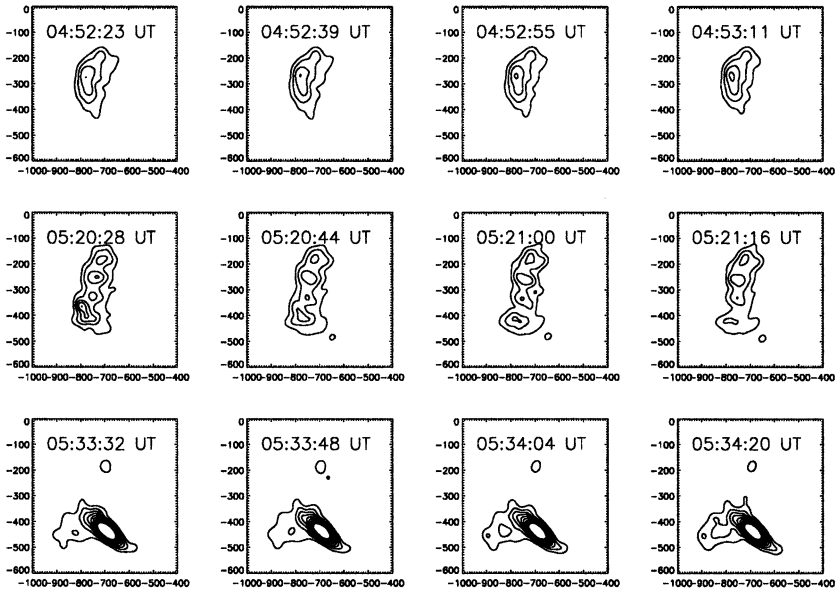

Figure 9. Contours of 16-s snapshots of the GMRT 1060 MHz emission. The center of these images is at S15 E46 and the field of view is $600'' \times 600''$. The restoring beam is $34'' \times 24''$. The contour levels are 0.1, 0.2, 0.3, 0.4, 0.5, 0.6, 0.7, 0.8, 0.9, and 1.0 times the flux at the largest peak, which occurs at 05:33 UT. We show three sets of 16-s snapshots starting at 04:52:23 UT, 05:20:28 UT, and 05:33:32 UT. These correspond to the three peaks of the 1060 MHz light curve (Figure 8). The emission at the peaks of 04:52 UT and 05:20 UT are from a NS oriented loop system, whereas the emission at the peak at 05:33 UT is from a NE–SW oriented loop. The brightness temperature of the emission at each of these peaks is $\lesssim 10^8$ K.

(see Figure 2) this provides concrete evidence for the complexity of the magnetic fields in the region from which the flare and CME were initiated.

4. Initiation of the Flare–CME Event: Analysis

Table I shows the time sequence of events leading to, and after the CME–flare initiation, with emphasis on the non-thermal emission. The third and fourth columns show the estimated height in $R_\odot$ from which the corresponding phenomenon is believed to be emanating. We employ the model of Aschwanden and Benz (1995) in calculating these heights. The third column shows the height assuming that the radio emission emanates at the fundamental plasma frequency ($s = 1$) while the height in the fourth column is calculated assuming that the radio emission emanates at the first harmonic of the plasma frequency ($s = 2$). The difference between the heights quoted in the third and fourth columns is relevant only for the non-thermal radio emission at 200, 500, and 1060 MHz.

Masuda *et al.* (1994) estimate that the hard X-ray emission at the top of the flaring loop originates at a height of around 18 000 km. We have used this number as

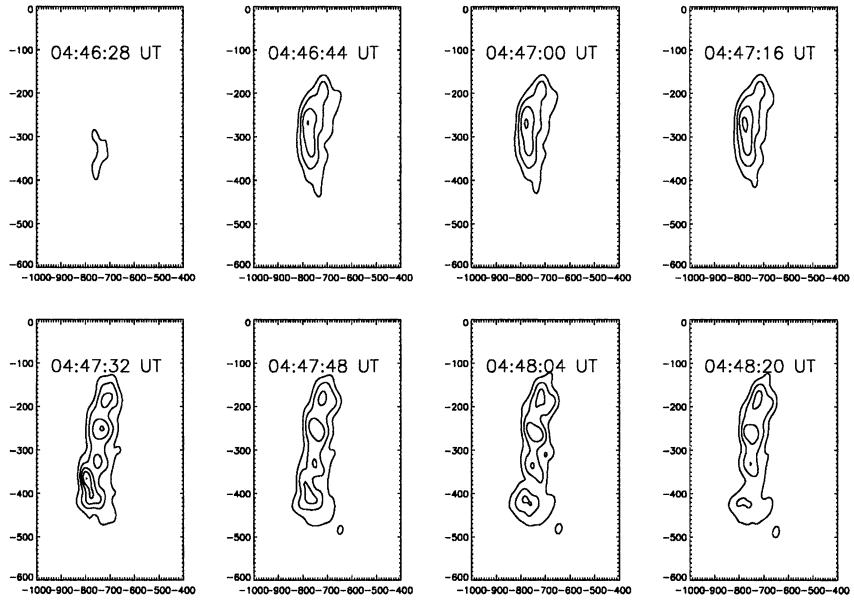

Figure 10. Snapshots at 16-s intervals near the rising edge of the first peak in the GMRT light curve. The contour levels and restoring beam are the same as those in Figure 9. It is clearly evident that the first peak of the 1060 MHz emission occurs between 04:47:32 and 04:47:48 UT.

a rough estimate of the height at which the hard X-ray flare (lower curve, Figure 1) originates. The fifth column gives the start time of the phenomenon, as evident from the corresponding light curve. We surmise that the non-thermal emission is a signature of magnetic reconnection, which provides sites for particle acceleration and consequent non-thermal emission. The start of non-thermal emission at a particular frequency therefore signals the start of reconnection processes at the height corresponding to that frequency.

The first sign of non-thermal activity associated with this event is the 200 MHz non-thermal emission quoted in item A (Table I). Detailed measurements of the trajectory of the prominence eruption associated with this event made by Kundu *et al.* (2003) reveal that the prominence is at $\sim 1.07\ R_{\odot}$ at 04:22 UT. The 200 MHz non-thermal emission peak of item A (Table I) occurs at 1.08 ($s = 1$) or 1.14 $R_{\odot}$ ($s = 2$), which is clearly above the prominence. This could be consistent with the predictions of the breakout model for solar eruptions (Antiochos, Devore, and Klimchuk, 1999), in which the first signature of eruption is the null-point reconnection above the central arcade which is going to erupt. According to this model, the central arcade rises slowly during the initial buildup stage, due to shearing at its footpoints, pushing the overlying constraining field lines and distorting the X-type null point (above the central arcade). Beyond a certain point, the current layer at the overlying null point becomes sufficiently thin so that ideal MHD evolution is no longer possible and reconnection sets in, so that the overlying constraining

TABLE I
Sequence of events in CME–flare initiation.

Item	Description	$R_\odot$ ($s = 1$)	$R_\odot$ ($s = 2$)	Start (UT)
A	200 MHz[1]	1.08	1.14	04:22
B	Lower envelope of drifting continuum[2]	1.186	1.33	04:48
C	410 MHz[3]	1.044	1.08	04:48
D	1060 MHz N–S source (1)[4]	1.02	1.04	04:48
E	Prominence eruption[5]			$\sim$04:48
F	X-ray flare[6]	1.02	1.02	04:49
G	500 MHz (2)[7]	1.037	1.067	04:50
H	1060 MHz N-S source (2)[8]	1.02	1.04	05:13
I	500 MHz (2)[9]	1.04	1.06	05:13
J	1060 MHz NE–SW source[10]	1.02	1.04	05:30
K	CME[11]	5	5	05:30

[1]Peak in fixed-frequency light curve from Hiraiso, Figure 6.
[2]Rapid increase in velocity of lower envelope of drifting continuum (Figures 4 and 5).
[3]Peak in fixed-frequency light curve from Learmonth, Figure 7.
[4]GMRT 1060 MHz data; Figures 8 and 10.
[5]NoRH 17 GHz data; Figure 3 and Kundu *et al.* (2003).
[6]GOES data; Figure 1, lower curve, and Masuda *et al.* (1994).
[7]Peak in fixed-frequency light curve from Hiraiso; Figure 6.
[8]GMRT 1060 MHz data; Figures 8 and 9.
[9]Fixed-frequency light curve from Hiraiso; Figure 6.
[10]GMRT 1060 MHz data; Figures 8 and 9.
[11]LASCO C2 data.

field lines connect to adjoining arcades. The measurements of Kundu *et al.* (2003) however reveal that the prominence had started rising well before 04:22 UT, the time at which the 200 MHz non-thermal emission peak of item A (Table I) occurs. This could be because the evolution of the null point above the central arcade prior to 04:22 UT was ideal, since the current layer was not thin enough for reconnection to set in. However, this does remain an open question.

The next noteworthy feature evident from Table I is the near-simultaneity of items B, C, D, E, F, and G. The 200, 410, 500, and 1060 MHz light curves exhibit peaks between $\sim$04:48–04:50 UT. The X-ray flare and the prominence eruption also take place in this time interval. Measurements of the prominence trajectory by Kundu *et al.* (2003) show that items B–G (Table I) occur well below the prominence. The near-simultaneous non-thermal emission at heights ranging from 1.02 to 1.18 $R_\odot$ could thus arise from a vertical current sheet below the erupting arcade. During this time interval, the lower envelope of the drifting continuum in

the HiRAS dynamic spectrum (see Figures 4 and 5) could represent the top of this vertical current sheet. The velocity of this feature increases abruptly at around 04:48 UT (right panel of Figure 5), as is evident from the increase in the curvature of the lower envelope of the drifting continuum around 04:48 UT (Figure 4). This could be taken to mean that the top of the vertical current sheet accelerates upward around this time. Our observations thus indicate that, during the interval 04:48–04:50 UT:

(1) A vertical current sheet spanning at least 1.02 to 1.18 $R_{\odot}$ exists (items B–G, Table 1).

(2) The top of the current sheet accelerates upward (Figure 5, right panel).

(3) The prominence eruption and X-ray flare occur.

The formation of a vertical current sheet under the erupting arcade is a feature of several flux rope models for CME initiation (e.g., Forbes, 1991; Lin and Forbes, 2000; Mikić and Linker, 1994; Amari *et al.*, 2000). Reconnection at the vertical current sheet allows the eruption to proceed in these flux rope models. The height of the flux rope undergoes a sudden jump as a result of the (equally sudden) formation of a current sheet underneath it (Lin *et al.*, 1998; Forbes, 2000). The formation of a vertical current sheet underneath the erupting arcade is also a feature of the breakout model, although it is a secondary process not integral to the breakout per se (Antiochos *et al.*, 1999; Klimchuk, 2000). In the breakout model, reconnection in the vertical current sheet results in an increase in the speed of the eruption. The strong heating associated with this current-sheet reconnection is manifested as the X-ray flare.

Items H, I, and J (Table I) are post-eruptive phenomena. In particular, the 1060 MHz emission from the NE–SW oriented GMRT source (item J) is most likely caused by flare accelerated electrons trapped in the NE-SW oriented loop system. This is manifested as type IV-like decimetric continuum emission on the Hiraiso dynamic spectrum.

5. Conclusions

We have presented some of the first GMRT observations of a solar eruption. We have used GMRT observations at 1060 MHz in conjunction with data from the NoRH, the Hiraiso solar observatory and LASCO to investigate the onset mechanism of a flare–CME event on 17 November 2001. We find evidence for reconnection above the erupting arcade that could be construed as evidence in favor of the magnetic breakout model. We find evidence for the formation of a vertical current sheet below the erupting prominence. An abrupt increase in the velocity of the top of the vertical current sheet is accompanied by the M2.8 X-ray flare and the prominence eruption. The features associated with the formation of the vertical current sheet are consistent with the predictions of several variants of flux rope CME initiation models, as well as the magnetic breakout model.

Acknowledgements

We thank the staff of the GMRT who made these observations possible. GMRT is run by the National Centre for Radio Astrophysics of the Tata Institute of Fundamental Research, India. We gratefully acknowledge the open data use policy of the Nobeyama Solar Radio Observatory, the Learmonth Radio Observatory and the Mount Wilson Observatory. SOHO is a project of international cooperation between NASA and ESA. This research has made use of the CME catalog generated and maintained by NASA and the Catholic University of America in cooperation with the Naval Research Laboratory. PS thanks Dr Kuniko Hori for kindly supplying detailed data from the Hiraiso spectrograph and Dr James Klimchuk for several useful discussions. We thank the anonymous referee for several critical comments on an earlier version of this manuscript that helped us substantially improve the interpretation of the observations. The work of MRK, SMW and VIG was supported by NASA grants NAG5-11872, NAG5-12860, and NSF grant ATM 9909809.

References

Amari, T., Luciani, J. F., Mikić, Z., and Linker, J.: 2000, *Astrophys. J.* **529**, L49.

Ananthakrishnan, S. and Pramesh Rao, A.: 2002, in R.K. Manchanda and B. Paul (eds.), Giant Meterwave Radio Telescope, *Proc. Int Conf. on Multicolour Universe*, TIFR, Mumbai, 233 pp. (Available at *http://www.gmrt.ncra.tifr.res.in/gmrt_hpage/Users/doc/doc.html*).

Antiochos, S. K., Devore, C. R., and Klimchuk, J. A.: 1999, *Astrophys. J.* **510**, 485.

Aschwanden, M. J. and Benz, A. O.: 1995, *Astrophys. J.* **438**, 997.

Forbes, T. G.: 1991, *Geophys. Astrophys. Fluid Dynamics* **62**, 15.

Forbes, T. G.: 2000, *J. Geophys. Res.* **105**, 23153.

Klimchuk, J. A.: 2001, in P. Song, H. Singer, and G. Siscoe (eds.), *Space Weather*, *Geophysical Monograph* **125**, 143.

Kundu, M. R. *et al.*: 2003, *Astrophys. J.*, submitted.

Lin, J., Forbes, T. G., Isenberg, P. A., and Démoulin, P.: 1998, *Astrophys. J.* **504**, 1006.

Lin, J. and Forbes, T. G.: 2000, *J. Geophys. Res.* **105**, 2375.

Masuda, S., Kosugi, T., Hara, H., Tsuneta, S., and Ogawara, Y.: 1994, *Nature*, **371**, 495.

Mikić, Z. and Linker, J.: 1994, *Astrophys. J.* **430**, 898.